Bulgarian Chemical Communications, Volume 55, Issue 3 (pp. 188-195) 2023 *DOI: 10.34049/bcc.55.3.5518*

Enhanced iodide uptake from aqueous solutions by silver-modified mesoporous SBA-15

F. Zahakifar[1], N. Karkhanei[2], J. Fasihi[1], H. Sepehrian[1*]

[1]*Nuclear Science and Technology Research Institute, Tehran, Iran*
[2]*Chemistry Department, Islamic Azad University, Saveh Branch, Saveh, Iran*

Received: July 24, 2022; Revised: July 18, 2023

In this work, mesoporous Ag-SBA-15 was prepared and its iodide adsorption from aqueous solutions was examined. The synthesized adsorbent was characterized by powder X-ray diffraction (XRD) and nitrogen adsorption-desorption. The impacts of several parameters such as pH, agitation time, temperature, initial iodide concentration, and competing anions have been also scrutinized in batch experiments. The adsorption capacity at pH=2.0 was high which decreased with increasing the pH value. The kinetics of iodide adsorption was in good agreement with the pseudo-first-order and second-order models. $\Delta H°$, $\Delta\Delta S°$, and $\Delta\Delta G°$ were 16.7 kJ.mol^{-1}, 0.11 J.mol^{-1}.k^{-1}, and -17.3 kJ.mol^{-1}, respectively. The results illustrated that the experimental data of the adsorption isotherm can be well described by the Langmuir model. The maximum adsorption capacity of Ag-SBA-15 was 312.5 mg.g^{-1}. The results indicated the high ability of Ag-SBA-15 to adsorb iodide.

Keywords: Mesoporous SBA-15; Surface modification, Impregnation, Silver; Iodide; Adsorption

INTRODUCTION

Today, environmental concerns arising from nuclear power plants have become a serious threat [1, 2]. The uranium fission in nuclear reactors may result in fission fragments which are usually unstable and radioactive [3-5]. These elements are easily soluble in the water, posing adverse effects on human health [6-8].

The 1986 Chernobyl nuclear disaster in Ukraine has raised concerns about releasing these elements. After the nuclear accident in Fukushima, the leakage of nuclear waste has become a serious concern [9].

Iodine is one of the crucial fission elements. Iodide isotopes have a half-life of 8 days to 1.6×10^7 years [10]. The thyroid collects iodide and there is a risk of damage to the body by radioactive iodide. Ref. [11] highlights the urge for the treatment of radioactive iodide in nuclear waste and its removal from water sources [12]. Iodide removal by adsorption methods is one of the effective techniques. In this regard, various adsorbents such as activated carbons [13], silver-impregnated sorbents [9], anion-exchange resins [14, 15], and activated carbon fibers [13] have been used to remove iodide from the aqueous solutions. However, most of these adsorbents have disadvantages such as small and irregular pore size, inaccessible pores, and low surface area which limits their use [16].

Mesoporous molecular sieves have gained increasing attention owing to their specific characteristics such as large pore size, high specific surface area, and excellent thermal and mechanical stability [17]. So far, mesoporous materials such as MCM-41, MCM-48, CMK-3, and CMK-5 have been employed to remove ions from wastewater [18].

Compared to the mentioned materials, the SBA-15 has a larger pore size and a thicker wall, which can significantly enhance thermal stability [19]. Therefore, SBA-15 can be a promising adsorbent for iodide. Functionalization can further increase the adsorption ability of SBA-15 toward ions.

Using functionalized SBA-15, several elements such as uranium [20], copper [21], and lead [22-24] have been adsorbed from aqueous solutions. Moreover, previous studies have shown that silver can well adsorb iodide [25-28]. Therefore, silver is expected to be a suitable material for functionalizing SBA-15 for better iodide uptake.

The main purpose of this paper was to prepare an SBA-15 impregnated with silver atoms and to use it as a novel iodide adsorbent. The impacts of several parameters such as pH, temperature, agitation time, initial concentration of iodide, ionic strength, and competing anions were also scrutinized in batch experiments. Iodide equilibrium adsorption data were analyzed using adsorption isotherms such as Langmuir, Freundlich and Temkin isotherms.

* To whom all correspondence should be sent:
E-mail: Hsepehrian@aeoi.org.ir

EXPERIMENTAL

Materials

The materials used to produce the Ag-SBA-15 adsorbents were all of analytical grade and purchased from Merck. P123 copolymer was obtained from Sigma-Aldrich. Sodium iodide was utilized to make the iodide-containing feed solution.

Apparatus

The prepared Ag-SBA-15 was characterized by powder X-ray diffraction (XRD) and nitrogen adsorption-desorption. The X-ray studies were performed using the Philips X'pert powder diffractometer system operating by Cu-Kα (λ = 1.541 Å) radiation. XRD analysis was performed from 1.5° to 100° (2θ) at a scan rate of 0.02° (2θ) s^{-1}. The nitrogen adsorption-desorption analysis was conducted by the Quantachrome NOVA model 2200e to measure specific surface area, total pore volume, and pore size. The concentration of iodide in the solutions was measured with an inductively coupled plasma-atomic emission spectrometer (ICP-AES, Varian, Liberty 150ax Turbo, Australia).

The zero charge point was determined by the pH drift method [29, 30]. A 0.01 $mol.L^{-1}$ KNO_3 was used as the inert electrolyte. The pH of test solutions was adjusted in the range of 2-10 using 0.01 $mol.L^{-1}$ HNO_3 and 0.01 $mol.L^{-1}$ KOH. 0.2 g of Ag-SBA-15 adsorbents was added to 50 mL of test solutions in glass tubes and equilibrated for 24 h. The final pH (pH_f) was measured after 24 h and plotted against the initial pH (pH_i). The point where the curve intersects the line $pH_i = pH_f$ was taken as the pH_{pzc}. The pH was measured by Schott CG841 pH-meter (Germany), which was calibrated before every measure.

Preparation of mesoporous silica SBA-15

According to the reported synthesis methods [16, 31-33], 0.8 g of P123 copolymer was added to 60 g of distilled water and 160 g of HCl (2 $mol.L^{-1}$) and stirred for 15 min at a rate of 130 rpm. Then, 3 g of tetraethyl orthosilicate (TEOS) was gradually added to the mixture and stirred for 20 h.

The produced precipitate was then placed in a Teflon container and kept at 90 °C for 24 h. After this time, a filtration operation was carried out on the precipitate using a Büchner funnel followed by rinsing with distilled water. The filtered precipitate was dried for 24 h in an oven at 50 °C. Finally, the precipitated sample was calcined in a furnace at 540 °C for 6 h to remove residual surfactants.

Preparation of mesoporous silica Ag-SBA-15

To impregnate the prepared adsorbent with silver, 1 g of SBA was added to 3 mL of a 1.20 $mmol.L^{-1}$ silver nitrate solution and stirred. It was then placed in an oven at 105 °C for 12 h to dry. Then 10 mL of 10 $mol.L^{-1}$ hydrazine hydrate was added to 1 g of product to convert silver ions to silver atoms. After one hour, the adsorbent was filtered and washed with sufficient distilled water and dried in an oven at 50 °C. The SBA-15 silicon porous adsorbent containing silver particles was named Ag-SBA-15.

Procedure of adsorption experiments

Batch experiments were carried out to investigate the iodide adsorption utilizing Ag-SBA-15 adsorbent. In these experiments, 25 mg of the adsorbent was mixed with 25 mL of iodide solution. The mixture of solution and adsorbent was shaken at the rate of 150 rpm utilizing a water bath shaker. The solution was filtered after the adsorption process. The iodide concentration in the solution was measured by ICP-AES. The adsorption percentage, adsorption capacity (q), and distribution coefficient (K_d) were calculated using the following equations:

$$\text{Adsorption (\%)} = \frac{(C_i - C_f)}{C_i} \times 100 \quad (1)$$

$$q = (C_i - C_f) \times \frac{V}{m} \quad (2)$$

$$K_d = \frac{(C_i - C_f)}{C_f} \times \frac{V}{m} \quad (3)$$

where C_i and C_f, V, and m are the initial and final concentrations of iodide (mg L^{-1}), solution volume (mL), and the mass of the adsorbent (g), respectively.

RESULTS AND DISCUSSION

Characterization of modified mesoporous adsorbent

The prepared Ag-SBA-15 adsorbent was characterized by XRD and BET techniques.

Nitrogen adsorption and desorption isotherms of SBA-15 and Ag-SBA-15 samples were investigated at 77 °K. Specific surface area and pore size distribution of adsorbent were obtained from BET and BJH equations, respectively [34-36]. The pore size distribution of samples is illustrated in Figure 1. This Figure confirms the mesoporosity of the adsorbent. The pore size distribution curve demonstrates a mean pore size of ~4 nm.

The pore size distribution curve also shows that the pore size distribution of Ag-SBA-15 was shifted to

slightly larger values since silver atoms filled the SBA-15 micro-pits.

The physical properties of SBA-15 and Ag-SBA-15 are presented in Table 1. The surface area, pore volume, and size of SBA-15 changed from 816 $m^2.g^{-1}$, 0.84 $cm^3.g^{-1}$, and 4.9 nm to 513 $m^2.g^{-1}$, 0.73 $cm^{-3}.g^{-1}$, and 4.61 nm upon silver impregnation. These changes are due to the entrance of silver atoms into the SBA-15 pores.

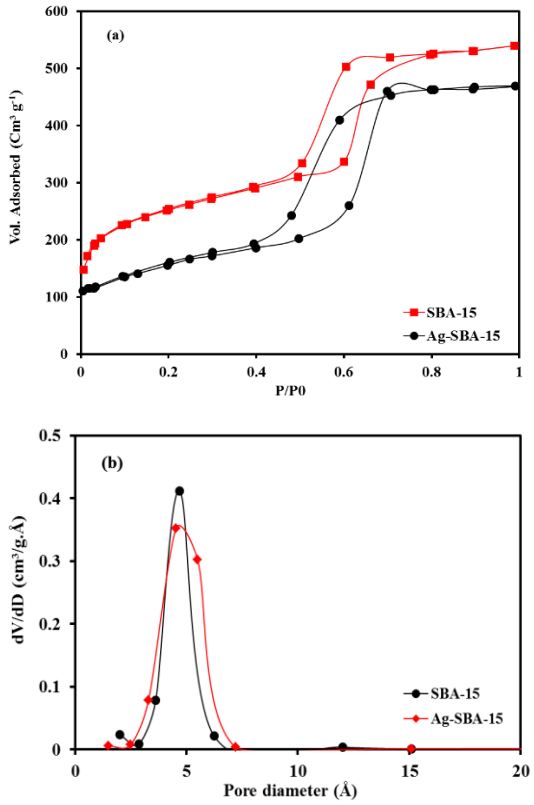

Figure 1. (a) Nitrogen adsorption and desorption isotherm and (b) Pore size distribution curve of SBA-15 and Ag-SBA-15 adsorbents

Table 1. Physical properties of SBA-15 and Ag-SBA-15 adsorbents

Sample	Pore volume (cm^{-3} g^{-1})	Specific surface area (m^2 g^{-1})	Average pore size (nm)
SBA-15	0.84	816	4.09
Ag-SBA-15	0.73	513	4.61

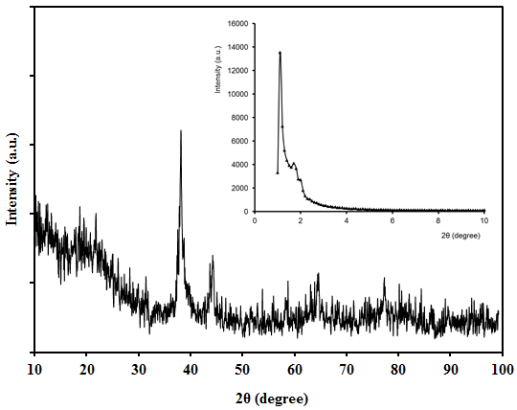

Figure 2. XRD pattern of Ag-SBA-15 adsorbent

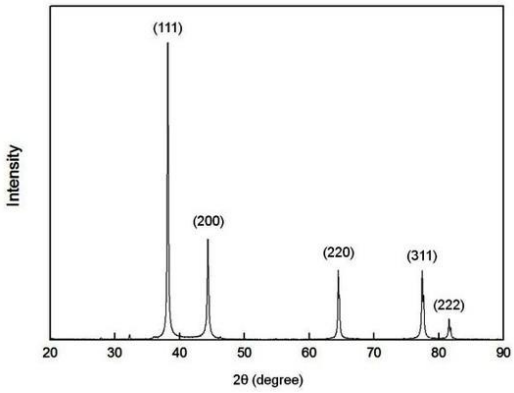

Figure 3. XRD pattern of silver nanoparticles [36]

The X-ray diffraction pattern of the Ag-SBA-15 is demonstrated in Fig. 2. As shown, its XRD pattern in 2θ = 2-10 is similar to that of mesoporous SBA-15, while the pattern in 2θ =10-100 confirms the presence of silver particles in the Ag-SBA-15 pores. The XRD pattern of silver nanoparticles prepared by Park *et al.* is in complete agreement with that of the Ag-SBA-15 (Fig. 3) [36]. Therefore, it is confirmed that silver atoms are present in the pores of the mesoporous SBA-15 without disturbing the structure of the mesoporous adsorbent.

Effect of acidity

The effect of acidity on iodide adsorption was studied in the pH range of 1-8. The results are demonstrated in Figure 4. At acidities less than 3, the iodide adsorption was favorable, while maximum iodide adsorption was obtained at pH = 2.

At low pH (pH<3), metallic silver is oxidized to silver ions on the adsorbent surface (Eq. 4). With the production of silver ions, the adsorbent surface becomes positively charged [37].

$$O_2(aq) + 4H^+(aq) + 4Ag^0(s) \rightarrow 4Ag^+(aq) + 2H_2O(l) \quad (4)$$

The pH_{pzc} of the Ag-SBA-15 was 4.0. At pH values lower than pH_{pzc}, the adsorbent possesses a positive surface charge. This behavior explains the higher adsorption of Ag-SBA-15 at pH <4.0. As the pH of the solution increased, the iodide adsorption decreased due to the rise in OH ions and their competition with iodide. Adsorption experiments were continued at an initial pH of 2.0.

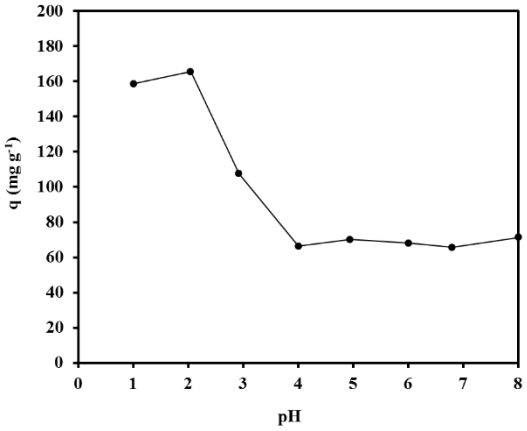

Figure 4. Effect of initial pH on iodide adsorption with Ag-SBA-15 (nitial pH: 1-8, agitation time 5 h, temperature: 25 °C, adsorbent: 25 mg, concentration: 1.2×10^{-2} M NaI, and solution volume: 25 mL).

Study of adsorption kinetics

The impact of agitation time on the iodide adsorption by Ag-SBA-15 was studied at 25 °C, as shown in Figure 5 (a). According to the results, iodide adsorption is a slow process and the adsorption rate increases with increasing time up to 24 hours and then reaches equilibrium. Other tests were performed for 48 h to achieve equilibrium.

Figures 5 (b) and 5 (c) show the graphs of pseudo-first-order and pseudo-second-order kinetics, respectively. The adsorption kinetics study demonstrated that the process agrees with the mentioned kinetic models. This means that the adsorption depends on the adsorbent surface and the concentration of iodide.

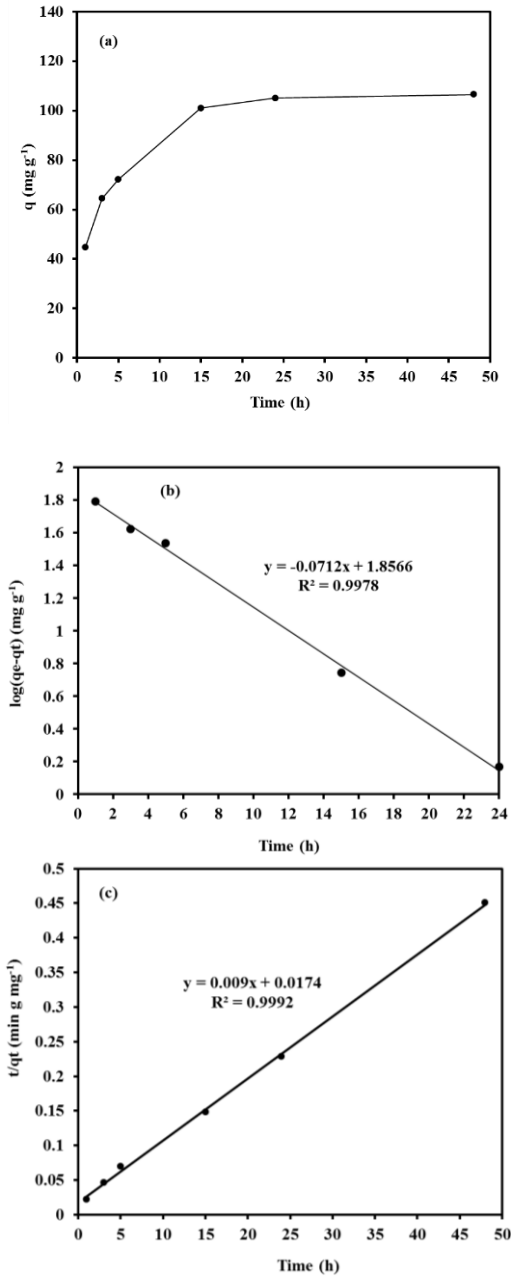

Figure 5. (a) Effect of agitation time on iodide adsorption with Ag-SBA-15; (b) pseudo-first-order kinetics (c) pseudo-second-order kinetics (initial pH: 2, temperature: 25 °C, adsorbent: 25 mg, concentration: 1.2×10^{-2} M NaI, and solution volume: 25 mL).

Effect of temperature

The impact of temperature on the iodide adsorption rate of Ag-SBA-15 was studied at 25 to 65 °C, as illustrated in Figure 6.

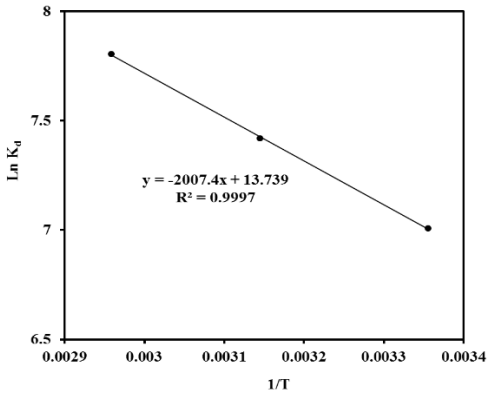

Figure 6. Effect of temperature on iodide adsorption with Ag-SBA-15 (initial pH:2, agitation time 48 h, adsorbent: 25 mg, concentration: 1.2×10^{-2} M NaI, and solution volume: 25 mL).

The mechanism of iodide adsorption can be determined by thermodynamic values. The thermodynamic values such as the change in Gibbs free energy (ΔG^o), adsorption enthalpy (ΔH^o), and entropy (ΔS^o) were obtained from the Van't Hoff equations [38, 39]:

$$\Delta G^0 = -RT \ln K_d \quad (5)$$

$$\ln K_d = \frac{\Delta H^0}{-(RT)} + \frac{\Delta S^0}{R} \quad (6)$$

where R and T (K) are the gas constant (8.314 J.mol^{-1}.K^{-1}) and the absolute temperature, respectively.

ΔH^o, ΔS^o, and ΔG^o were obtained, 16.7 kJ.mol^{-1}, 0.11 J.mol^{-1}.k^{-1}, and -17.3 kJ.mol^{-1}, respectively, implying an endothermic and spontaneous adsorption process. Therefore, with increasing temperature, the adsorption of iodide on the adsorbent will increment.

Iodide adsorption isotherm

The isotherm experiments were performed with an initial concentration of iodide between 5 and 300 mg L^{-1} at pH 2 for 48 h. Langmuir, Freundlich, and Temkin are common isotherm models that describe the nature and mode of adsorption of ions onto the adsorbent. The mathematical expressions of these models are expressed in the following equations [40-43]:

$$q_e = \frac{q_L K_L C_e}{1 + K_L C_e} \quad (7)$$

$$q_e = K_F C_e^{1/n} \quad (8)$$

$$q_e = \frac{RT}{b_T} \ln(K_T C_e) \quad (9)$$

where q_e and q_L are adsorption capacity at equilibrium and Langmuir maximum adsorption capacity, respectively. K_L, K_F, and b_T are Langmuir, Freundlich, and Temkin model constants. K_T is the Temkin isotherm equilibrium binding constant. The n denotes the deviation from the linearity of adsorption, and C_e is the equilibrium concentration of ions.

Experiments were performed with various concentrations of iodide to study the adsorption isotherm. Figure 7 (a) demonstrates the iodide adsorption isotherms on the Ag-SBA-15 adsorbent. The Langmuir, Freundlich and Temkin linear adsorption models are illustrated in Figures 7 (b) and 7 (d), respectively. The parameters of these models are shown in Table 2. As seen, the experimental data of the adsorption isotherm are well described by the Langmuir model. Therefore, uniform and homogeneous adsorption on the Ag-SBA-15 adsorbent can be considered [44-47].

The K_F and 1/n in the Freundlich model are indicators of adsorption capacity and adsorption power. A less than one 1/n value shows normal adsorption [48]. The maximum adsorption capacity of iodide on Ag-SBA-15 adsorbent was calculated as 312.5 mg g^{-1}.

Effect of coexisting anions

The impact of coexisting anions on iodide adsorption with Ag-SBA-15 was also investigated as shown in Figure 8. For this purpose, a solution of 1.2 mol.L^{-1} sodium iodide was prepared containing different concentrations of fluoride and chloride. The results demonstrated that iodide adsorption decreased with raising the concentration of the fluoride and chloride which declined the adsorption capacity to about 65 mg g^{-1}.

So far, several studies have been performed on iodide adsorption using various adsorbents [37, 49-51], as summarized in Table 3. It is observed that the amount of iodide adsorbed by the present adsorbent is much higher than by other adsorbents, and the q_{max} value increased to 312.5 mg g^{-1}. The high adsorption efficiency is probably due to the high affinity of silver and the top surface area of Ag-SBA-15 adsorbent compared to other adsorbents.

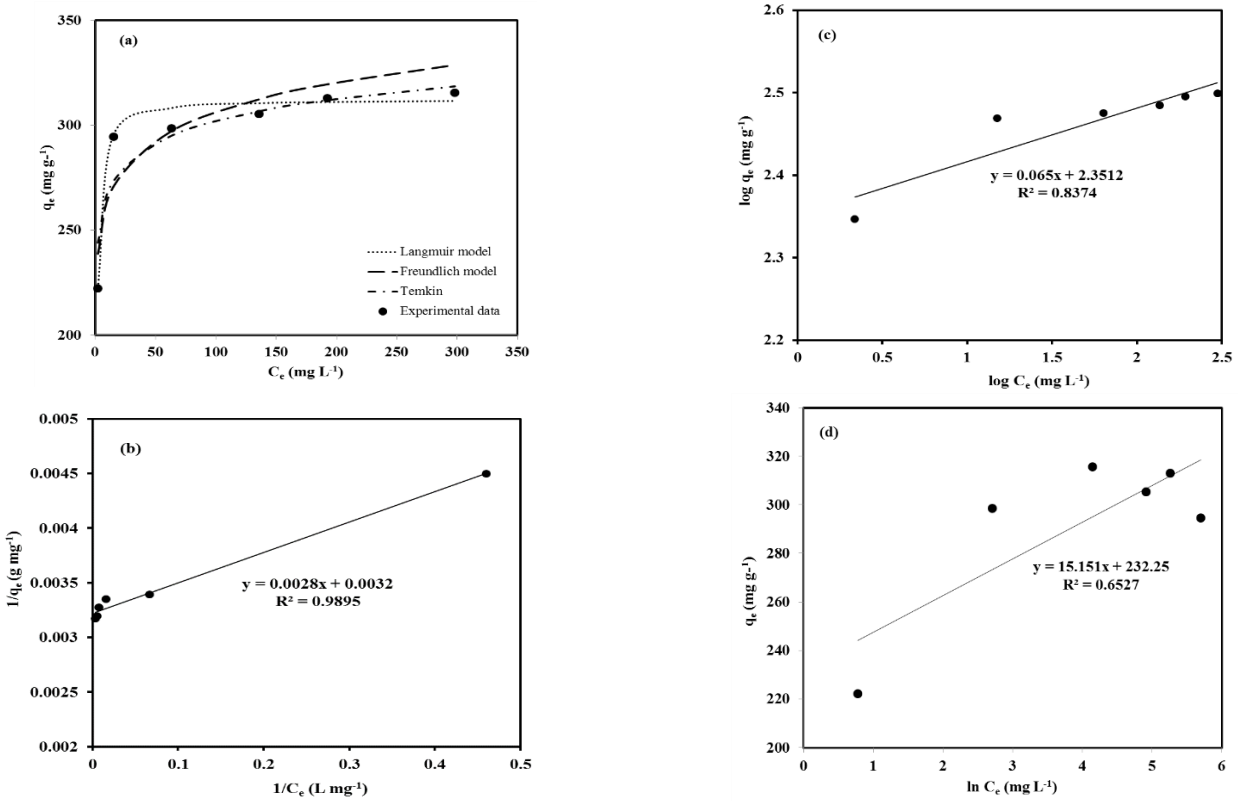

Figure 7. (a) Iodide adsorption isotherms on Ag-SBA-15; (b) Langmuir, (c) Freundlich; (d) Temkin linear model (initial pH: 2, agitation time 48 h, temperature: 65 °C, adsorbent: 10 mg, solution volume: 20 mL

Table 2. Parameters of the Langmuir, Freundlich and Temkin models for iodide adsorption

Model	Parameters		
Langmuir	R^2	K_L(L mg^{-1})	q_{max}(mg g^{-1})
	0.989	1.14	312.5
Freundlich	R^2	K_F (mg g^{-1} mg^m L^m)	1/n
	0.837	224.49	0.065
Temkin	R^2	b_T	K_T (L g^{-1})
	0.65	163.53	4591359

Table 3. Comparison of iodide adsorption by Ag-SBA-15 with other adsorbents

Adsorbent	Initial iodide conc. (mg L^{-1})	Iodide adsorption		Ref.
		%	mg g^{-1}	
Duolite A-116	510	50	-	[49]
Mg-Al-(NO_3) LHD[a]	342	59	-	[50]
CaALG-AgCl composite[b]	-	-	139.7	[51]
AgAC[c]	1-200	-	18.2-19.5	[37]
Ag-MCM-41	88-352	34-95	166.7-238.1	[52]
Ag-SBA-15	113-445	33-98	222.3-312.5	This work

[a]Layered double hydroxide
[b]Calcium alginate-silver chloride composite
[c]Silver-impregnated granular activated carbon

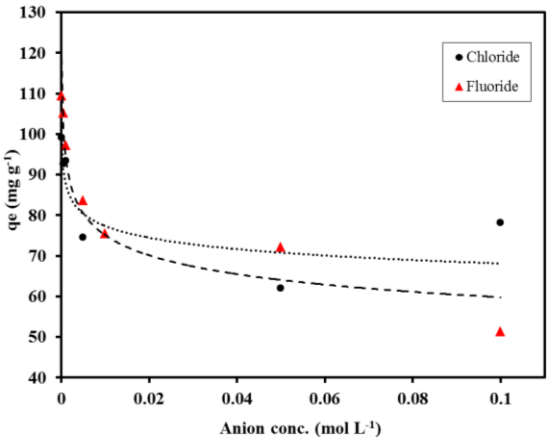

Figure 8. Effect of concentration of fluoride and chloride ions on iodide adsorption on Ag-SBA-15 adsorbent (initial pH: 2, agitation time 48 h, temperature: 25 °C, adsorbent: 25 mg, solution volume: 25 mL).

CONCLUSIONS

In this research, a new adsorbent (Ag-SBA-15) was prepared by impregnating SBA-15 with silver atoms and its adsorption behavior for iodide was studied. The adsorbent was characterized by powder XRD and nitrogen adsorption-desorption. The results indicated the loading of silver nanoparticles on the mesoporous SBA-15.

The adsorption behavior of iodide on Ag-SBA-15 was also examined. The adsorption capacity was very high at pH=2.0 and decreased with enhancing pH value. The results illustrated that the adsorption reaction is endothermic and spontaneous and follows the pseudo-first-order and second-order kinetic models. Also, experimental data were well described by the Langmuir model. The maximum adsorption capacity of iodide onto Ag-SBA-15 was found to be 312.5 mg g^{-1}. These results illustrated that Ag-SBA-15 has the appropriate ability for adsorption of iodide from aqueous solutions.

Data Availability: Some or all data, models, or codes that support the findings of this study are available from the corresponding author upon reasonable request.

REFERENCES!

1. M. Sadiq, F. Wen, *Nuclear Engineering and Technology*, **54** (10), 3672 (2022).
2. S. Venturi, *Juvenis Scientia*, **8** (2), 5 (2022).
3. F. Zahakifar, A. Charkhi, M. Torab-Mostaedi, R. Davarkhah, *Journal of Radioanalytical and Nuclear Chemistry*, **316** (1), 247 (2018).
4. F. Zahakifar, A. Charkhi, M. Torab-Mostaedi, R. Davarkhah, *Radiochimica Acta*, **106** (3), 181 (2018).
5. F. Zahakifar, A. Charkhi, M. Torab-Mostaedi, R. Davarkhah, A. Yadollahi, *Journal of Radioanalytical and Nuclear Chemistry*, **1** (2018).
6. P. Kumar, B. Kumar, D. Singh, in: Hazardous Waste Management, Elsevier, 2022, p. 289.
7. T. S. Rao, S. Panigrahi, P. Velraj, in: Microbial biodegradation and bioremediation, Elsevier, 2022, p. 419.
8. F. Zahakifar, A. Keshtkar, E. Nazemi, A. Zaheri, *Radiochimica Acta*, **105** (7), 583 (2017).
9. A. Bo, S. Sarina, Z. Zheng, D. Yang, H. Liu, H. Zhu, *Journal of Hazardous Materials*, **246**, 199 (2013).
10. J. Livingood, G. Seaborg, *Physical Review*, **54** (10), 775 (1938).
11. M. Eisenbud, Y. Mochizuki, A. S. Goldin, G. R. Laurer, *Science*, **136** (3514), 370 (1962).
12. L. Szente, É. Fenyvesi, J. Szejtli, *Environmental Science & Technology*, **33** (24), 4495 (1999).
13. O. B. Yang, J. C. Kim, J. S. Lee, Y. G. Kim, *Industrial & Engineering Chemistry Research*, **32** (8), 1692 (1993).
14. N. Hiromichi, K. Hiroshi, M. Nobuaki, S. Hiroshi, S. Akira, N. Masashi, D. Yuu, Google Patents, 1967.
15. S. K. Glenn,(ed.), Google Patents, 1960.
16. X. Wang, G. Zhu, F. Guo, *Annals of Nuclear Energy*, **56**, 151 (2013).
17. C. Kresge, M. Leonowicz, W. J. Roth, J. Vartuli, J. Beck, *Nature*, **359** (6397), 710 (1992).
18. M. Gao, G. Zhu, C. Gao, *Energy and Environment Focus*, **3**, 219 (2014).
19. D. Zhao, J. Feng, Q. Huo, N. Melosh, G. H. Fredrickson, B. F. Chmelka, G. D. Stucky, *Science*, **279**, 5350 (1998).
20. Y. Liu, L. Yuan, Y. Yuan, J. Lan, Z. Li, Y. Feng, Y. Zhao, Z. W. Chai, , *Journal of Radioanalytical and Nuclear Chemistry*, **292** (2), 803 (2012).
21. Da'na, A. Sayari, *Chemical Engineering Journal*, **166** (1), 445 (2011).
22. S. Wang, K. Wang, C. Dai, H. Shi, J. Li, *Chemical Engineering Journal*, **262**, 897 (2015).
23. Y. Liu, Z. Liu, J. Gao, J. Dai, J. Han, Y. Wang, J. Xie, Y. Yan, *Journal of Hazardous Materials*, **186** (1), 197 (2011).
24. V. Hernández-Morales, R. Nava, Y. Acosta-Silva, S. Macías-Sánchez, J. Pérez-Bueno, B. Pawelec, *Microporous and Mesoporous Materials*, **160**, 133 (2012).
25. F. Forstmann, W. Berndt, P. Büttner, *Physical Review Letters*, **30** (1), 17 (1973).
26. K. W. Chapman, P. J. Chupas, T. M. Nenoff, *Journal of the American Chemical Society*, **132** (26), 8897 (2010).
27. C. Mathew, M. Majali, S. Balakrishnan, *Applied Radiation and Isotopes*, **57** (30), 359 (2002).

28. T. R. Thomas, B. A. Staples, L. P. Murphy, (eds.), Google Patents, 1978.
29. Y. Yang, Y. Chun, G. Sheng, M. Huang, *Langmuir*, **20** (16), 6736 (2004).
30. A. Aziz, M. S. Ouali, E. H. Elandaloussi, L. C. De Menorval, M. Lindheimer, *Journal of Hazardous Materials*, **163** (1), 441 (2009).
31. M. Kruk, M. Jaroniec, C. H. Ko, R. Ryoo, *Chemistry of Materials*, **12** (7), 1961 (2000).
32. S. Vashnia, H. Tavakoli, R. Cheraghali, H. Sepehrian, *Desalination and Water Treatment*, **55** (5), 1220 (2015).
33. Y. Wang, B. Zibrowius, C.-M. Yang, B. Spliethoff, F. Schüth, *Chemical Communications*, **1**, 46 (2004).
34. M. Hayati-Ashtiani, *Particle & Particle Systems Characterization*, **28** (3-4), 71 (2011).
35. E. P. Barrett, L. G. Joyner, P. P. Halenda, *Journal of the American Chemical Society*, **73** (1), 373 (1951).
36. E. J. Park, S. W. Lee, I. C. Bang, H. W. Park, *Nanoscale Research Letters*, **6** (1), 223 (2011).
37. J. S. Hoskins, T. Karanfil, S. M. Serkiz, *Environmental Science & Technology*, **36** (4), 784 (2002).
38. X. Huang, N.-Y. Gao, Q.-l. Zhang, *Journal of Environmental Sciences*, **19** (11), 1287 (2007).
39. M. Sekar, V. Sakthi, S. Rengaraj, *Journal of Colloid and Interface Science*, **279** (2), 307 (2004).
40. S. Chen, Y. Qi, J. J. Cossa, S. I. D. S. Dos, *Progress in Nuclear Energy*, **117**, 103 (2019).
41. I.-K. Jung, Y. Jo, S.-C. Han, J.-I. Yun, Science of the Total Environment, 2019, p. 135814.
42. A. Yusoff, M. Salimi, S. Gopinath, M. Abdullah, E. Samsudin, *Materials Chemistry and Physics*, **241**, 122337 (2020).
43. A. Mehdinia, S. Heydari, A. Jabbari, *Materials Chemistry and Physics*, **239**, 121964 (2020).
44. F. Zahakifar, A. R. Keshtkar, M. Talebi, *Progress in Nuclear Energy*, **134**, 103642 (2021).
45. F. Zahakifar, A. R. Keshtkar, M. Talebi, *Journal of Radioanalytical and Nuclear Chemistry*, **327** (1), 65 (2021).
46. F. Vaziri Alamdarlo, G. Solookinejad, F. Zahakifar, M. Rezvani Jalal, M. Jabbari, *Journal of Water and Wastewater; Ab va Fazilab (in Persian)*, 2021.
47. F. V. Alamdarlo, G. Solookinejad, F. Zahakifar, M. R. Jalal, M. Jabbari, *Journal of Radioanalytical and Nuclear Chemistry*, **329** (2), 1033 (2021).
48. A. Dada, A. Olalekan, A. Olatunya, O. Dada, *IOSR Journal of Applied Chemistry*, **3** (1), 38 (2012).
49. R. Lokhande, P. Singare, S. Parab, *Radiochemistry*, **50** (6), 642 (2008).
50. L. Kentjono, J. Liu, W. Chang, C. Irawan, *Desalination*, **262** (1-3), 280 (2010).
51. H. Zhang, X. Gao, T. Guo, Q. Li, H. Liu, X. Ye, M. Guo, Z. Wu, Colloids and Surfaces A: Physicochemical *and Engineering Aspects*, **386**, (1-3), 166 (2011).
52. N. Karkhanei, H. Sepehrian, R. Cheraghali, *Desalination and Water Treatment*, **56** (11), 3096 (2015).